“KMOS3D Survey: data release and final survey paper”

Wisnioski et al. 2019
ApJ 886. 124
arXiv:1909.11096

Presenter: K. Kushibiki

Contents (in 29 pages)

Abstract

Completed KMOS^{3D} survey

IFS of 739, $\log(M_*/M_\odot) > 9$ galaxies at $0.6 < z < 2.7$

→ Population-wide census of …

- Kinematics
- Star formation
- Outflows
- Nebular gas condition

On & off SFMS through spatially resolved & integrated properties with Hα (6563), [NII]λλ6548,6584, [SII]λλ6716,6731

Abstract

Hα detection

- Detect for 91% of galaxies on MS, 79% overall
- Deep survey allow us to detect galaxies with SFR below 1 $M_{\odot}yr^{-1}$
- Resolve 81% of detected galaxies with ≥ 3 resolution elements
- Detection fraction is a strong function of both color and offset from MS, with the detected and non-detected galaxies exhibiting different SED

Dust attenuation correction

- From comparison between Hα and UV+IR SFR, dust attenuation correction may be underestimated by 0.5 dex at $\log(M_*/M_{\odot})$

Kinematics

- High rotation dominated fraction of 77% for the full samples
- Rotation-dominated fraction is a function of both stellar mass and redshift with the strong evolution for galaxies with $\log(M_*/M_{\odot}) < 10.5$

1. Introduction
Importance of NIR-IFS & First Generation Results

Near-infrared integral field unit (NIR-IFU) spectrograph

→ Spatially & spectrally resolved rest-optical nebular emission lines of z ~ 1-3 galaxies (Hα, Hβ, [NII] [SII], [OIII], [OII])

→ 2D mapping of kinematics, star formation, and physical condition of ISM

Results of these properties supported "the equilibrium growth scenario" "fairly continuous gas accretion" vs "internal dynamical processes"

First Generation NIR-IFU (VLT/SINFONI, Keck/OSIRIS, Gemini/NIFS)

→ Importance of internal process in the early growth of massive galaxies

- Rotating, yet turbulent disks among massive SFGs, which have irregular and clumpy appearance (Genzel+2006, etc.)
- Launching site and role of galactic wind powered by SF and AGN (Nesvadba+2008, etc.)

for a couple hundred z~1-3 galaxies with seeing res. → need more samples !!

1. Introduction
KMOS & KMOS^{3D}

KMOS (K-band Multi-Object Spectrograph) at VLT

- 24 individual IFUs with a 2″.8 x 2″.8 FoV
- Seeing-limited mode with the pixel scale 0″.2
- Spectral resolution R ~ 4000

→ Expand NIR-IFU surveys to much larger, homogeneous, more complete samples

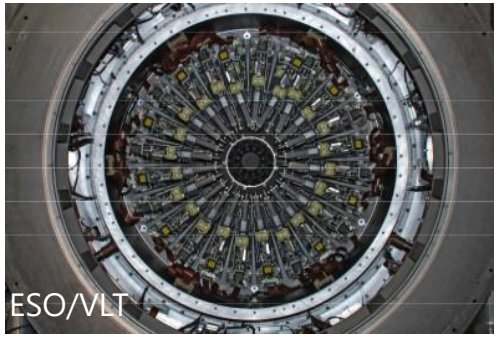

KMOS^{3D}

- 75-night survey of Hα+[NII]+[SII] emissions
- 739 galaxies at z ~ 0.6-2.7

Main goals

- Robust census of resolved properties across the entire massive galaxy population
- Track consistently the evolution from peak of comic-SFR to local

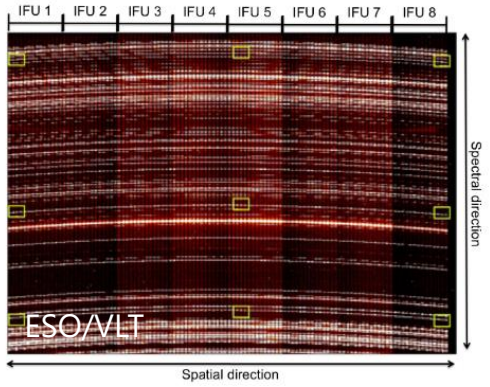

1. Introduction
KMOS^{3D} Sample Selection

Basic concept

1. Homogeneous coverage in redshift and galaxy stellar mass
2. The use of the same spectral diagnostics across the redshift range
3. Deep integration to map faint, extended line emission

↓

3D-HST

- Well characterized parent sample (detection, redshift)
  → reducing bias towards blue, rest-UV bright galaxies
- Overlap with CANDELS → multi-wavelength imaging

Selection criteria

1. Stellar-mass and K-band magnitude cuts
2. Reliability of the redshift
3. Emission lines of interest falling in NIR atmospheric windows and away from bright sky lines

1. Introduction
KMOS^{3D} main results

Main science drivers

- dynamics
- angular momentum
- structure of galaxies
- galactic outflows
- chemical enrichment
- quenching of star formation activity

Key science results (previous papers)

- robustly confirmed **the majority (≳70%) of rotating disks** among z ~ 1-3 SFGs **with greater turbulence** (Wisnioski+2015, Übler+2019)
- **angular momentum** distribution of high-z SFGs **reflects that of their host dark matter halo** (Burkert+2016)
- high-z disks become increasingly **baryon-dominated** out to z ~ 2.5 (Wuyts+2016b, Lang+2017, Übler+2017, Genzel+2017)
- trends with stellar mass and SFR of **the properties of ionized gas outflows** and **the high duty cycle > 50% of nuclear AGN-driven winds** at $\log(M_*/M_\odot) \gtrsim 11$ (Genzel+2014, Förster Schreiber+2019)
- new constraints on **metallicity scaling relations** and evidence in support of typical **flat gas-phase oxygen abundance gradients** (Wuyts+2014, 2016a)
- shed new light **on dense core formation and quenching** (Belli+2017, Wisnioski+2018)

2. Sample Selection
Parent sample of KMOS^{3D}

3D-HST grism Treasury Survey

- within COSMOS, GOODS-S, UDS fields visible from the VLT
- 0.7 < spec-z or grism-z < 2.7 (spec-z: 36% of targeted)
  → main emission line fall within KOMS YJ(0.7-1.1), H(1.2-1.8), K(1.9-2.7)
  (referred as z~1, z~1.5, z~2.0, respectively)

Homogeneous set of SED: from X-ray to far-IR and radio (including CANDELS survey for optical and NIR data)

→ Global properties by Wuyts+2011b method
(optical-8μm SED fit by BC03, solar-metallicity, Calzetti+2000, constant/exponentially declining SFRs)

- Stellar mass
- SFR (SED fits or rest-UV+IR luminosities)
- global dust extinction correction

Resolved information derived from high resolution optical-NIR imaging

Environment catalog from Fossati+2017

2. Sample Selection
Selection Criteria

- K-band magnitude < 23 AB and stellar mass > $10^9 M_\odot$
  No cut involving SFR and/or color
  → reduce bias toward most actively SFG and/or bluest galaxies
- Grism quality flag (Momcheva+2016) for galaxies with grism-z
  → doesn't change the distribution of samples from parent sample
  (Stellar mass, MS offset, rest-UVJ, offset from mass-size relation)
  By using grism-z objects, largely reducing bias towards bluer, star-forming objects

Effect of K-band magnitude cut

- Reduce 90% mass completeness limit, $\log(M_*/M_\odot)$~9.6, 10.2, 10.6 for z~1, 1.5, 2.0
- remove sub-MS objects

Fig 1.

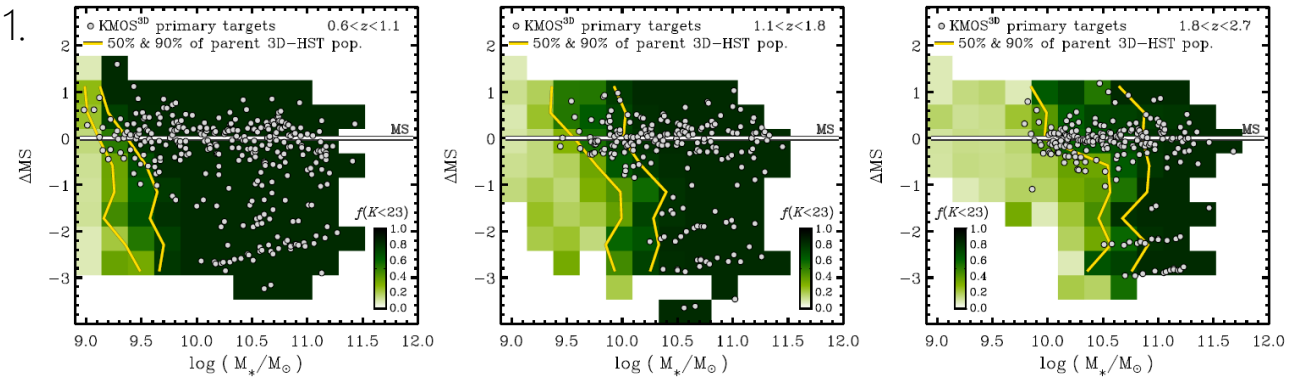

2. Sample Selection
Selection Criteria (cont'd)

Sky emission & absorption

"visibility"
=Inverted sky emission × atmospheric transmittance × PDF of lines
> 0.5 for Hα and [NII]λ6584

PDF of lines

- spec-z objects: σ=400km/s Gaussian
- grism-z objects: σ=1000 km/s Gaussian

→ remove ~70% of possible targets

Visual inspection of 3D-HST 2D spectrum

→ 142 galaxies were removed

because of …

- low-S/N in the grism
- low grism coverage on the basis that grism spectrum would not significantly improve the phot-z estimate

3. Observation

75 nights, Oct. 2013 – Apr. 2018

Seeing

- 70% of data having PSF FWHM < 0.55″

Observing time

- multiple pointings for high S/N
- Some with the longest obs. times > 14 h
  - low surface brightness feature
  - low-levels of star-formation
  - passive galaxies
- median: 5.0, 8.5, 8.7 h for each z range

Fig 2.

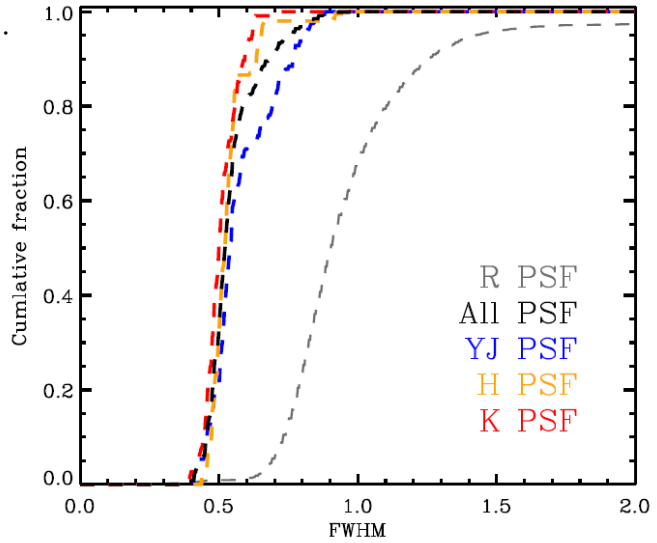

Fig 3.

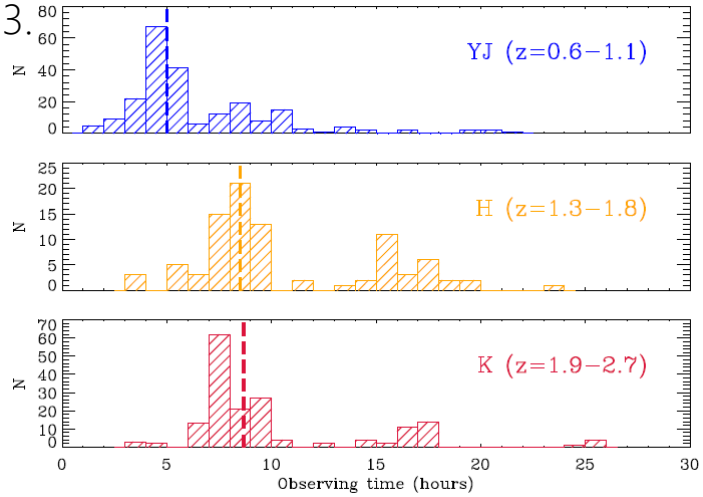

3. Observation

Observation methods

- OSOOSO dithering
- subpixel/pixel shift for bad pixels
- 3 IFUs for "PSF star" (one per detector)

Dark & Bright night

- Dark: YJ obs. , Bright: K obs.
- A moon distance < 30 degrees cause the error on the background
  1.7, 1.4, and 1.0 factor increase for YJ, H, K

Calibration data

- Darks, lamp flats, arcs → at the end of each night
  No sky flats during observation runs because of the persistence of detectors
- Standard stars for telluric transmission & flux calibration
  → at the start & end & between pointings

4. Data Reduction

SPARK software ver. 1.3.5 & custom PYTHON & IDL scripts

4.1. Detector-level correction

- Read-out ch-dependent bias level
- Altering column noise (ACN)

} Corrected by bias removal with reference pixels

→ Left significant spatial non-uniformity around their perimeter

- Picture frame noise (Rauscher 2013,2015) ← due to drifts in bias voltage (±10 counts in extreme case)
  → Using =7500 dark frames to estimate the correlation between the median reference pixel value and each pixels in science frame
  →estimate and remove the residual picture frame noise

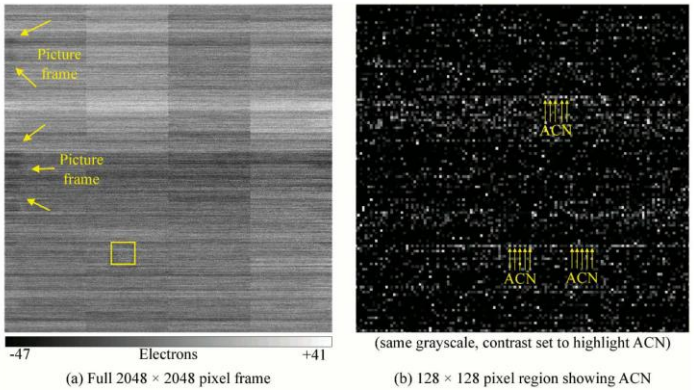

Fig. 1.— (a) Each NIRSpec H2RG has 2048×2048 pixels. This reference corrected full frame CDS dark is typical for NIRSpec's H2RGs when driven by the T ∼ 40 K SIDECARs. The standard deviation is about $\sigma_{\rm read} = 14\ e^-$ rms. The four video outputs are visible as thick 512×2048 pixel stripes. The horizontal banding is caused mostly by $\sim 1/f$ drifts in the bias voltages generated by the SIDECAR. The yellow arrows point to picture frame noise. There is more picture frame noise on the opposite side of this image that we did not highlight to avoid obscuring it. In (b), we expand the yellow 128×128 pixel box to show ACN. Because the NIRSpec detector subsystem was tuned to minimize ACN, it is not easy to see. One of the downloadable examples has been tuned to more clearly show ACN.

Rauscher 2015

4. Data Reduction

4.2. Sky subtraction and heliocentric correction

Performed external to SPRAK in two step

1. Simple O-S subtraction
2. Removal of sky line residuals
   with modified ZAP Principal Component Analysis (PCA) sky subtraction code
   → reduce residual of sky features
   compare standard deviation of spectra

Heliocentric correction in the range ± 30 km/s

4.3. Illumination correction

Rotator angle dependent illumination correction
→ residual non-uniformity ~ ± 3%

Fig 4.

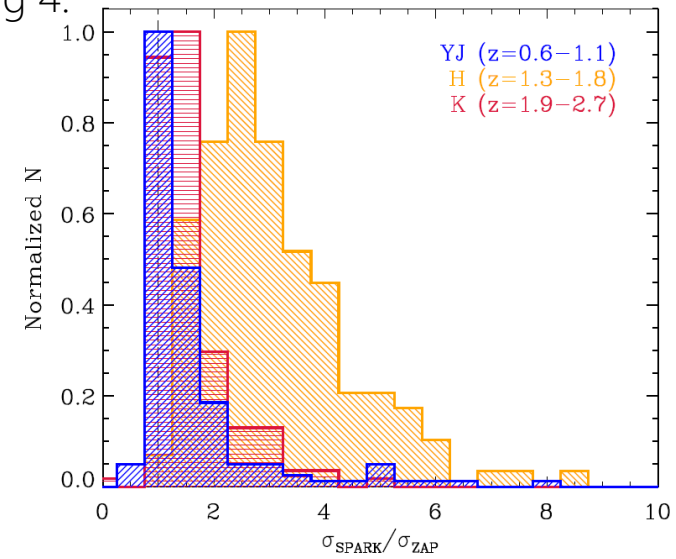

4. Data Reduction

4.4. Flux calibration

A0, B, G star from Hipparcos Catalog with known IR mag
→ telluric transmission correction & flux calibration (for each detector)

- Photometric Zero point in AB system
  Mean counts in 2MASS, J, H, K filters in 1D spectrum
  → zero point (std = 0.19, 0.39, 0.26 mag over full survey)
- Correction for the variation of observing conditions
  Total flux in the PSF stars of each frame
  vs Median flux of it in the 3 science frames observed closest in time
- Make a spectrum in flux
  - Airmass correction
  - Zero point is applied

  → Offsets from known magnitudes

YJ	H	K
-0.09 ± 0.13	-0.07 ± 0.18	-0.04 ± 0.19

Fig 5.

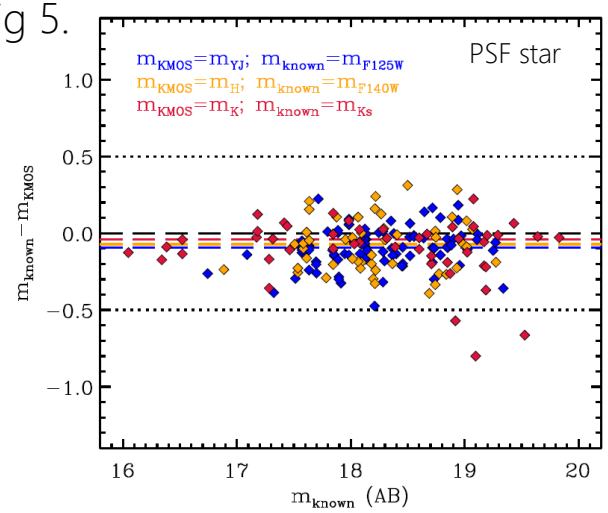

4. Data Reduction

4.5. Background subtraction

Remove residual spatial non-uniformity driven by channel-to-channel variation (4 distinct output channels for each IFU)

→ Model the background as …
channel dependent + spatially- and spectrally-uniform component

→ Background correction: a few$\times 10^{-21} \pm 5 \times 10^{-20}$ erg/s/cm^2/AA
(median surface brightness at re = 10^{-20} erg/s/cm^2/AA order)

For bright sources, overestimate background $\lesssim$ 10%

4.6. Combined cubes and astrometric alignment

- 3σ clipping average without bad or failed data(6.6%)
- Astrometric shift
  - Average measured offset from the 3 PSF stars (in short timescale)
  - Compare partial combined datacube to HST image(closest band, FoV, binning)
    → make centroid variable and the best fit is the one minimizing chi-squared
    (98.6%(730/739): continuum image, 4 cubes: Hα, 6 cubes: fainter than Ks=22.3)
    → median shift ~ 1 KMOS pixel, 10%of the cubes > 2 pix

4. Data Reduction

4.7. Associated PSF images

- Moffat fit with PSF star image → centroid & total flux
- normalized total flux as unity → allowing different stars to be combined
- shifted and combined with Swarp

→Obtain PSF image for each object

4.8. Spectral resolution

- Arc lamp cube
  → Fit Gaussian profile to the arclines in each spaxel, Average the spectral resolution at the wavelength
  → 4th order polynomial fitting of spec. res.

$$R = RES\ COEFF0 + RES\ COEFF1 \times \lambda_{obs} + RES\ COEFF2 \times \lambda_{obs}^2 + RES\ COEFF3 \times \lambda_{obs}^3 + RES\ COEFF4 \times \lambda_{obs}^4$$

- Sky cube (from the same raw data as science cubes)
  → correct the difference of reduction between arc cube and science cube by adjusting 0th term

Fig 6.

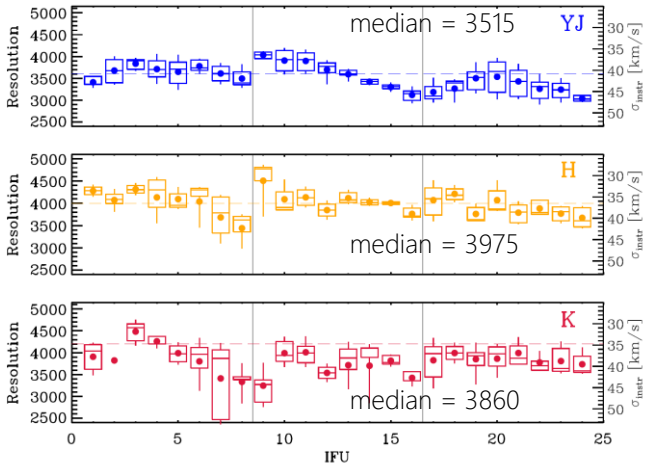

4.9. Bootstrap cubes

Complement the default noise cube and provide more realistic noise estimates

5. Integrated Hα Properties

Detect Hα emission for 581 of the targeted galaxies
→ 79%

z	1.0	1.5	2.0
mass range [log($M_*/M_\odot$)]	9.00-11.43	9.44-11.45	9.79-11.68

5.1. Detection fractions

Relation to redshift

	detection fraction
36% with a spec-z	84%
64% with a grism-z	76%

	detection fraction
z ~ 1.0	77% (245/319)
z ~ 1.5	79% (159/201)
z ~ 2.0	81% (177/219)

Standard deviation of redshift difference (Brammer+2008)

$$\sigma_{\mathrm{NMAD}} = 1.48c \times \mathrm{median}\left|\frac{\Delta z - \mathrm{median}(\Delta z)}{(1+z_{\mathrm{kmos}})}\right| \quad , \Delta z = z_{best} - z_{kmos}$$

	all	with spec-z	with grism-z	with grism-z & below MS
σ_{NMAD}	463 km/s	155 km/s	1020 km/s	1546 km/s

Fig 7.

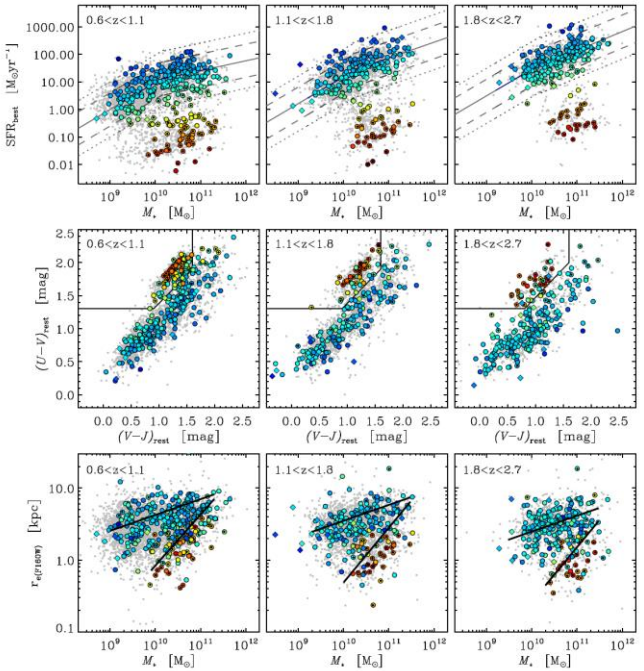

Fig 8.

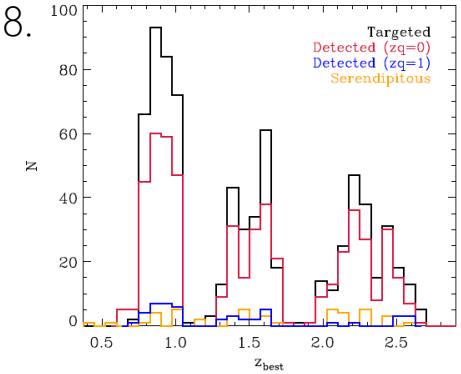

5. Integrated Hα Properties

5.1. Detection fraction (cont'd)

Relation to MS offset/galaxy color

detection fraction	ΔMS > -0.85 (on & above MS)	ΔMS < -0.85 (below MS)
All	91% (541/592)	27% (40/147)
z ~ 1.0	90% (219/243)	34% (26/76)
z ~ 1.5	93% (148/160)	27% (11/41)
z ~ 2.0	92% (174/189)	10% (3/30)

Non-detections below the MS don't correlate with magnitude or exposure time

Fig 9.

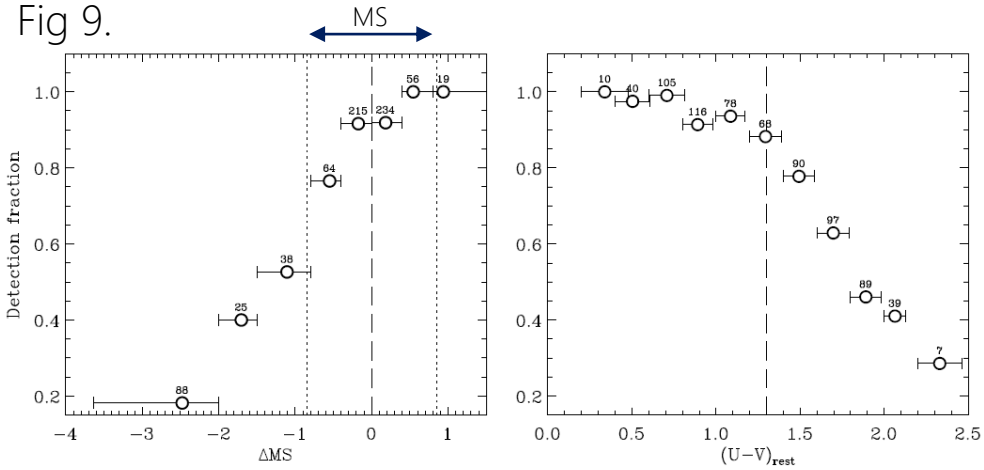

Relation to SED

- SFG (ΔMS > -0.85)
  - detected galaxies (det): identical to 3D-HST
  - undetected galaxies (undet): redder
    →strong dust extinction
    median IR/UV higher by 3.5x than det sample
- Quiescent (ΔMS < -0.85)
  - no difference between det and undet: redder, old
  - det sample: rejuvenation/gas outflows, shocks (Belli+2017)

Fig 10.

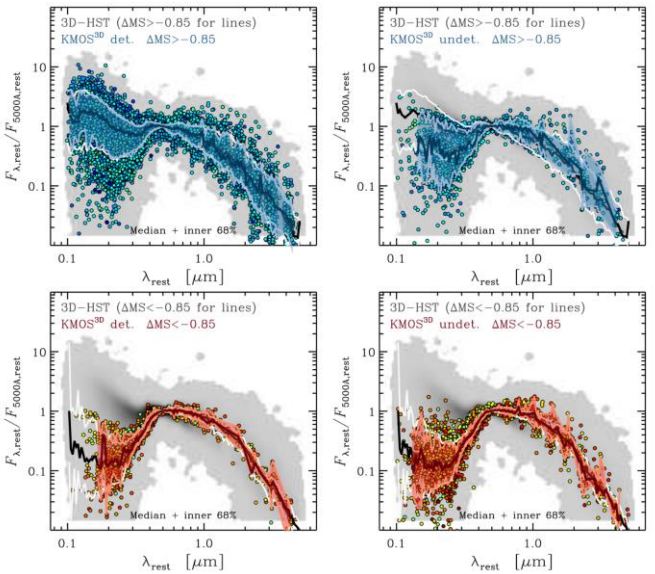

5. Integrated Hα Properties

5.1.1. Non-detections

Small number of galaxies with blue color and on-MS are not detected

→Larger uncertainties and misidentification of the redshift

cf) Hα of 41 galaxies are detected at > 10,00 km/s from the expected redshift

5.1.2. Serendipitous galaxies

46 galaxies, $0.4<z<2.6$, $8.4<\log(M_*/M_\odot)<10.9$

Majority of them are single emission line detection & part of them out of FoV

5.1.3. Final sample distributions

a more homogeneous coverage in mass and redshift

Fig 11.

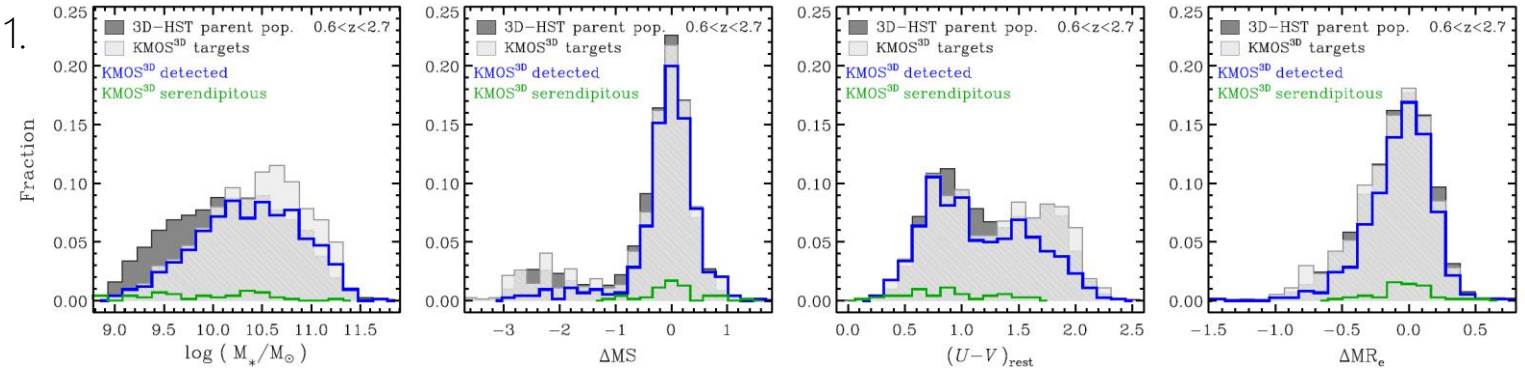

5. Integrated Hα Properties

5.2. Integrated spectra and Hα fluxes

- 1″.5 radius aperture at the center of continuum
- Continuum subtraction (real galaxy continuum + sky residual)
  - Mask channels within 1000 km/s of strong emission line
  - Calculate the median of each spectrum in 30 pixel wide window

  → linear interpolation and subtraction (+ mask spikes)
- Hα+[NII]λλ6548,6563 fitting
  - Multi-line fit ([NII] position and width tied to Hα)
    or Single Gaussian fit (for spectrum where [NII] is weak/contaminated)
    → For majority, multi-line fit is adopted (visual inspection/χ^2)
  - Errors are estimated by bootstrap cubes
- Aperture correction (Based on Wilman+2019 and structural params from HST F160W image)
  - Mock 2D Hα exponential profile
    with the same axis ratio and r_e = 1.19 x r_e(F160W)
- Some with high-velocity wings
  → two component (narrow/wide) fitting (strong gas outflow)
- [NII]: 70% (66, 74, 80% for $\log(M_*/M_\odot)$= 9.5-10.5, 10.0-11.0, 10.5-11.5: mass-metallicity)

5. Integrated Hα Properties

Fig 12.

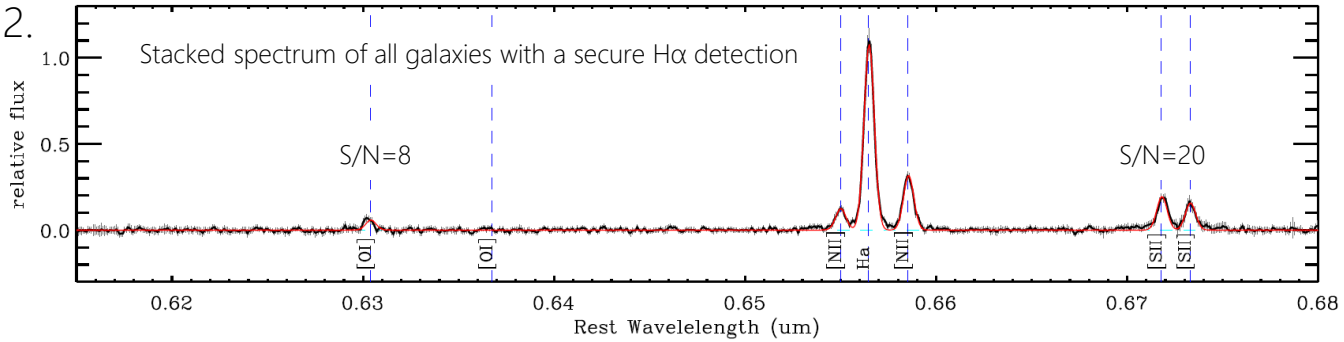

5.3 SFR comparisons

$$\mathrm{SFR}_{\mathrm{H}\alpha} = 4.65\times10^{-42} L_{\mathrm{H}\alpha}\, 10^{-0.4A_{\mathrm{extra}}}\, 10^{-0.4A_{\mathrm{cont}}} \quad \left(A_{\mathrm{extra}} = (0.9A_{\mathrm{cont}} - 0.15A_{\mathrm{cont}}^2) \quad A_{\mathrm{cont}} = 0.82A_{\mathrm{v,SED}}\right)$$

I think -0.4A should be +0.4A. Chabrier IMF, Calzetti+2000 curve

A_{extra} is a correction term for nebula emission (Wuyts+2013)

Comparison with UV+IR or SED SFRs

- on-MS: Good agreement
- below MS: $SFR_{SED} < SFR_{H\alpha}$ →SED models (e.g. SFH) (Belli+2017)
- above MS: $SFR_{phot} > SFR_{H\alpha}$ →dust correction and/or "starburst"

Fig 13.

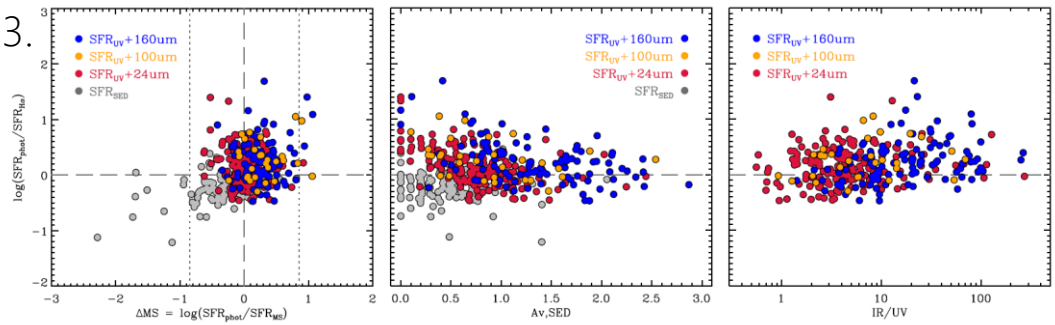

6. Resolved Hα Properties

6.1. Spatial Ha fitting

LINEFIT (Davies+2011)

- Intrinsic Gaussian convolved with a line profile representing the spectral resolution
- Uncertainties determined by 100 Monte Carlo simulation

→ Peak, position, width of Gaussian → Hα flux, velocity, velocity dispersion

- Mask including pixels with S/N>2, velocity and velocity dispersion error<100 km/s

Visual inspection for low S/N region

6.2. Kinematic parameters

Fig 14.

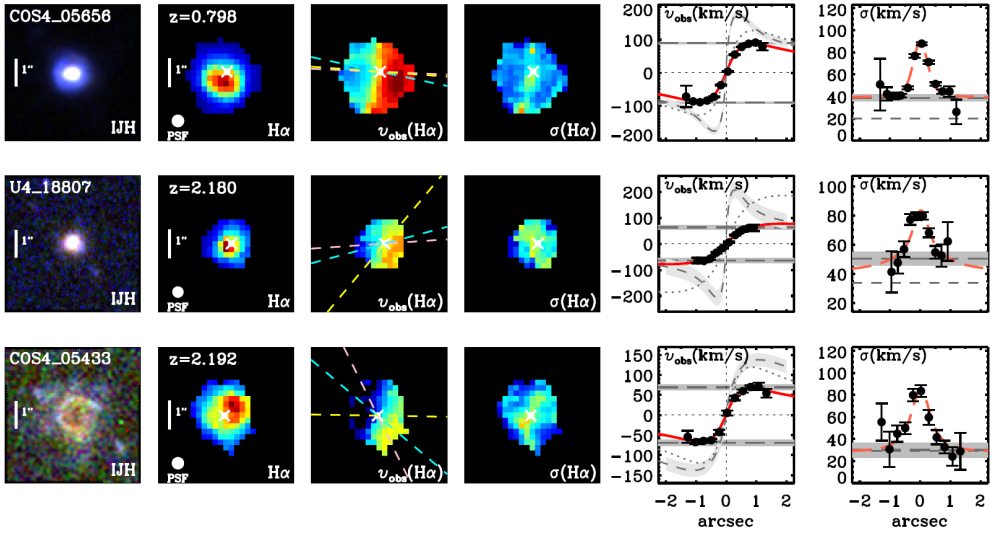

Kinematic axis
→ Line created by the positive and negative nodes
Define positive (negative) nodes as the highest(lowest) 5% of spaxels in the velocity maps

Kinematic center
→ half-way points between the nodes

6. Resolved Hα Properties

6.2. Kinematic parameters (cont'd)

Velocity and velocity dispersion profile along kinematic axis

Emission line fitting within aperture with diameter = FWHM of PSF

Criteria for including resulting fits

- S/N > 2
- the difference between successive velocity points < 150km/s
- Error on velocity δV_{xy} < 25 [km/s], on velocity dispersion $\delta \sigma_{xy}$ < 100 [km/s]

Maximum radius r_{kin} is defined by the farthest spaxel satisfying above criteria

Number of resolution elements

>3 elements for 81% of detected galaxies

Comparable in 3 bands (redshift ranges)
(marginally low in YJ by below-MS samples)

Out to ~2r_e in 60% of detected galaxies,
~3r_e in 30% of them
→ beyond where change in slope and flattening of velocity-curve

Fig 15.

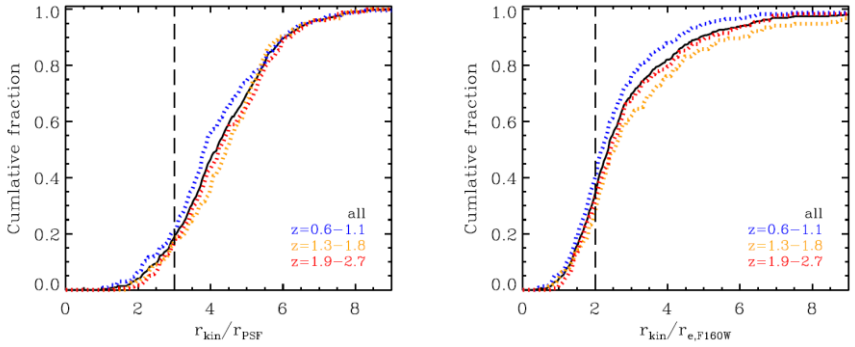

6. Resolved Hα Properties

6.2. Kinematic parameters (cont'd)

Observed velocity and velocity dispersion

- Observed velocity v_{obs}: the average of the absolute value of the minimum and maximum velocity
- Velocity dispersion σ_0: the weighted mean of all the data points from 1D velocity dispersion profile at > 0.75 x $|r_{kin}|$
  → Velocity dispersion in disk galaxies
  Apply regardless of kinematic type. → Disk fraction

From Fig 14.

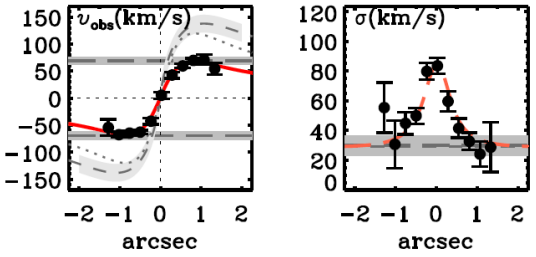

Effect of beam smearing

Correct with Burkert+2016 method

- Based on the intrinsic size of the galaxy, stellar mass, inclination, observed PSF size
- Agree with the result from correction based on full forward modelling

→ Beam smearing correction factor = median 1.36, (1.08-1.97)

However, since Hα size is greater than H-band size,
factor calculated from H-band size may be overestimated.

7. Analysis

7.1. Evolution of disk fraction

Wisnioski+15(W15): the fraction of "rotation-dominated" and "disk-like" of 83, 71%
→ Large sample and high S/N data are crucial to characterize disk fraction at any redshift and its evolution
→ KMOS3D full sample

5 disk criteria based on W15 (1, 2: rotation dominated, all: disk)

1. The Hα velocity map exhibits a continuous velocity gradient along a single axis
2. $v_{rot}/\sigma_0 > \sqrt{3.36}$
3. The position of the steepest velocity gradient is coincident with the peak of velocity dispersion within the uncertainties (~1.6pix)
4. For inclined galaxies (q<0.6) the photometric and kinematic axes agree
5. The position of the steepest velocity gradient is coincident with the KMOS continuum center within the uncertainties

Evolution z~2.3 to z~0.9
→ result of the evolving $\frac{v_{rot}}{\sigma_0}$
→ driven by the evolution of σ_0 (Übler+2019)

this paper

Table 2
% of galaxies satisfying disk criteria

Criteria:	1,2	1,2,3	1,2,3,4	1,2,3,4,5
$10.0 < \log(M_*/M_\odot) < 11.75$				
Full Sample	79%	65%	64%	59%
$z \sim 1.0$	91%	73%	70%	66%
$z \sim 1.5$	79%	68%	68%	65%
$z \sim 2.0$	70%	56%	56%	49%

W15

Table 1
% of galaxies satisfying disk criteria

Criteria:	1,2	1,2,3	1,2,3,4	1,2,3,4,5
Full Sample	83%	73%	71%	58%
$z \sim 1$	93%	78%	78%	70%
$z \sim 2$	74%	68%	64%	47%

7. Analysis

7.1. Evolution of disk fraction (cont'd)

As a function of stellar mass and its evolution

log($M_*/M_\odot$)=9.5-10.5 mass bin: the largest evolution
↔ log($M_*/M_\odot$)= 10.5-11.75 mass bin: shallower evolution

Rotation dominated fraction (v/σ >1 for comparison)
→ Agree with previous results

Caveat

1. Hα emission is probed to larger radii
2. Method of analysis
3. Slit-based analysis lead to high σ

Comparison with Illustris-TNG50
→ Qualitatively agree both in trends with mass and cosmic time

Table 3
% of galaxies satisfying disk criteria

Criteria:	1,2	1,2,3	1,2,3,4	1,2,3,4,5
$9.0 < \log(M_*/M_\odot) < 11.75$				
Full Sample	77%	61%	60%	55%
$z \sim 1.0$	87%	67%	65%	61%
$z \sim 1.5$	72%	57%	57%	54%
$z \sim 2.0$	69%	56%	55%	48%
$10.5 < \log(M_*/M_\odot) < 11.75$				
Full Sample	85%	72%	71%	66%
$z \sim 1.0$	88%	75%	74%	70%
$z \sim 1.5$	86%	75%	75%	72%
$z \sim 2.0$	81%	66%	66%	58%
$9.5 < \log(M_*/M_\odot) < 10.5$				
Full Sample	73%	54%	52%	49%
$z \sim 1.0$	91%	66%	62%	60%
$z \sim 1.5$	66%	49%	49%	46%
$z \sim 2.0$	58%	46%	45%	39%
$9.0 < \log(M_*/M_\odot) < 9.5$				
Full Sample	…	…	…	…
$z \sim 1.0$	63%	47%	47%	42%
$z \sim 1.5$	…	…	…	…
$z \sim 2.0$	…	…	…	…

Fig 17.

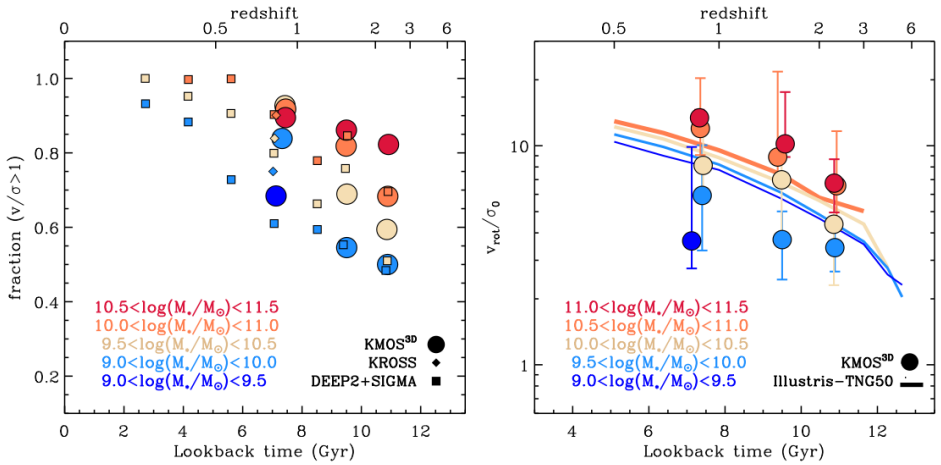

7. Analysis

7.1. Evolution of disk fractions (cont'd)

Rotation fraction
→ Constraints on the duty cycle of the processes perturbing rotational motions such as accretion event, internal processes(?), and interaction

From high rotation dominated fraction (and disk-like distribution of Hα, stellar light and mass)

- Major merger play a minor role in setting galactic structure observed at z~1-3
- Disk is largely preserved or regrown on short timescale as indicated by numerical simulations of gas-rich systems (Martin+2018, etc.)

7.2. Environmental effects on axis misalignment

Interaction can cause changes in the distribution of angular momentum
→ Misalignment of the kinematic and photometric axis

Only resolved and $0.2<q_{F814W}<0.8$ galaxies for accurate phot-axis

$\delta_{0.75}$: galaxies in an aperture of 0.75Mpc radius (Fossati+2017)

→ No difference and samples are classified as "central" in catalog

→ Miss any signatures of misalignment present in "satellite" galaxies

→ Compare stellar and gas kinematics/ High gas fraction make misalignment short-lived

Fig 18.

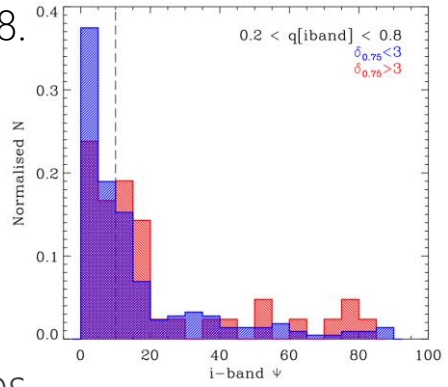

8. Data Release

Data cubes (FITS format)

- Science, noise, , exposure map, PSF image, and bootstrap cubes
- First time to implement a PCA approach to background subtraction in a large near-IR dataset → reduce background noise by a factor of 2
- 20% flux calibration accuracy
- (Release 1″.5 radius aperture Hα fluxes for 581 detected galaxies)

Catalog (FITS binary data table)

Table 5
Keywords for the released data table

Keyword	Description
ID	KMOS3D ID with field and 3D-HST v4 catalog object ID
FIELD	Field identifier; COS=COSMOS, GS=GOODS-SOUTH, U=UDS
ID_SKELTON	Object ID in 3D-HST v4 catalog (Skelton et al. 2014)
ID_TARGETED	KMOS3D ID when targeted, with field and 3D-HST (v2 or v4 catalog) object ID
FILE	Associated datacube in fits format
FLAG_PRIMARYTARG	1 = targeted as a primary KMOS3D target, 0 = serendipitous galaxy detection within IFU of a primary target
FLAG_ADDGALDET	1 = additional galaxy detected in the IFU of the primary target, 0 = no additional galaxy detected
FLAG_SEGMENTATION	1 = possible issues with photometry and derived parameters resulting from over or under segmentation, 0 = no issues identified with segmentation map
FLAG_ZQUALITY	1 = redshift/identification is uncertain, 0 = redshift is secure −1 = Non-detection
RA	Right ascension
DEC	Declination
Z_TARGETED	Best known redshift at time of observations
OBSBAND	Observing band
EXPTIME	Total exposure time (minutes)
PSF_FWHM	FWHM of PSF using Moffat model, minor axis (arcsec)
Z	Measured redshift from KMOS3D observations, -9999. if not detected
SPEC_RES	Estimated spectral resolution from arc and OH sky lines as described in Section 4.8
M_KS	Apparent Ks magnitude (AB)
RF_U	Rest frame absolute U-band magnitude (AB)
RF_V	Rest frame absolute V-band magnitude (AB)
RF_J	Rest frame absolute J-band magnitude (AB)
SFR	SFR from ladder of SFR indicators in $M_\odot$ yr^{-1} assuming a Chabrier (2003) IMF (see Wuyts et al. (2011b,a) - Section 2.2.3)
SFR_TYPE	SFR indicator of SFR 5 = SFR_UV+160um; 4 = SFR_UV+100um; 3 = SFR_UV+70um; 2 = SFR_UV+24um; 1 = SFR_SED
LMSTAR	Stellar mass derived from SED modeling following Wuyts et al. (2011b), using the FAST (Kriek et al. 2009) fitting code, Bruzual & Charlot (2003); Chabrier IMF; solar metallicity; Exponentially declining SFH with tau > 300 Myr; 0 < Av < 4; 50 Myr < age_since_onset, SF < age_universe
SED_AV	Dust attenuation towards V-band derived from SED modeling
RHALF	CANDELS H-band major axis effective radius (arcsec)
RHALFERR	error on CANDELS H-band major axis effective radius (arcsec)
Q	CANDELS H-band axis ratio
QERR	error on CANDELS H-band axis ratio
FLAG_HSOURCE	Source of Rhalf, Rhalferr, Q, Qerr: 1 = H-band fit from van der Wel et al. (2012); 2 = H-band fit from Lang et al. (2014)

ID	R.A.	Decl.	$z^a_{\rm best,orig}$	$K_{\rm AB}$ (mag)	Band	Exposure time^b (min)	PSF FWHM^c (arc sec)	R^d
COS4_00779	150.10114	2.1906323	0.92133	19.77	*YJ*	230	0.585	3682
COS4_00937	150.12886	2.1932354	0.87830	19.07	*YJ*	230	0.585	3160
COS4_00970	150.14334	2.1926434	0.79940	19.23	*YJ*	285	0.585	3430
COS4_01351	150.14261	2.1969705	0.85380	19.72	*YJ*	285	0.585	3604
COS4_01598	150.11681	2.1967461	1.02223	20.91	*YJ*	290	0.585	…

ID	$\log(M_*)$ ($M_\odot$)	$\rm SFR^a_{phot}$ ($M_\odot$ yr^{-1})	SFR type^b	$U_{\rm rest}$ (mag)	$V_{\rm rest}$ (mag)	$J_{\rm rest}$ (mag)	A^d_v	r_e[F160W]^e (arc sec)	q^f	flag^g
COS4_00779	10.85	16.46	2	-20.57	-22.26	-23.52	0.3	1.053	0.772	2
COS4_00937	11.17	14.59	5	-20.80	-22.62	-24.10	0.7	0.640	0.835	2
COS4_00970	11.04	0.87	1	-20.33	-22.34	-23.77	0.6	0.385	0.497	2
COS4_01351	10.73	57.40	5	-20.28	-21.82	-23.40	1.7	1.119	0.256	2
COS4_01598	10.50	0.74	1	-17.97	-20.18	-22.20	1.5	0.478	0.192	2

ID	$z^a_{\rm kmos}$	$z^b_{\rm q}$	$f^c_{\rm H\alpha}$ (10^{17} erg s^{-1} cm^2)	apperture correction	$\sigma_{\rm int}$ (km s^{-1})	Serendipitous flag^d
COS4_00779	0.92430	1	0±0	0±0	0±0	0
COS4_00937	0.87789	0	0±0	0±0	0±0	0
COS4_00970	0.82045	0	0±0	0±0	0±0	0
COS4_01351	0.85345	0	0±0	0±0	0±0	0
COS4_01598	…	0	0±0	0±0	0±0	0

9. Summary

Future Prospect

Near infrared IFS studies of z>1 galaxies have typically limited …

- medium resolution (R~ 2000-4000)
- narrow wavelength range covering only single emission line complexes

Future IFS instrument

- higher spectral and spatial resolution
  - ERIS/VLT; Davies+2018
  - GIRMOS/Gemini; Sivanandam+2018
- broader wavelength coverage
  - NIR-SPEC/JWST; Closs+2008
  - MIRI/JWST;
  - GMTIFS/GMT; Sharp+2016

→ Provide insight into small-scale motion, 10 km/s, of the ionized gas
Map the spatially varying ISM conditions